

ORIGINAL ARTICLE

Electrically driven, phosphor-free, white light-emitting diodes using gallium nitride-based double concentric truncated pyramid structures

Seung-Hyuk Lim¹, Young-Ho Ko^{1,2}, Christophe Rodriguez^{1,3}, Su-Hyun Gong¹ and Yong-Hoon Cho¹

White light-emitting diodes (LEDs) are becoming an alternative general light source, with huge energy savings compared to conventional lighting. However, white LEDs using phosphor(s) suffer from unavoidable Stokes energy converting losses, higher manufacturing cost, and reduced thermal stability. Here, we demonstrate electrically driven, phosphor-free, white LEDs based on three-dimensional gallium nitride structures with double concentric truncated hexagonal pyramids. The electroluminescence spectra are stable with varying current. The origin of the emission wavelength is studied by cathodoluminescence and high-angle annular dark field scanning transmission electron microscopy experiments. Spatial variation of the carrier injection efficiency is also investigated by a comparative analysis between spatially resolved photoluminescence and electroluminescence.

Light: Science & Applications (2016) 5, e16030; doi:10.1038/lsa.2016.30; published online 12 February 2016

Keywords: indium gallium nitride; light-emitting diodes; phosphor-free; three-dimensional structures; white color

INTRODUCTION

Group III-nitride semiconductor materials have been widely used in various optoelectronic devices, including light-emitting diodes (LEDs), laser diodes, and photodetectors. With technological advances in group III-nitride semiconductors^{1–3}, white LEDs using phosphor(s) that replace existing lighting sources have already been commercialized. However, phosphor-free white light sources are still in demand due to the drawbacks of using phosphor, such as Stokes energy conversion loss, high manufacturing cost, and reduced thermal stability of the phosphor-based LEDs^{3,4}. Therefore, to achieve phosphor-free broadband LEDs, two-dimensional (2D) film^{5–7} and three-dimensional (3D) gallium nitride (GaN) structures^{8–12} have been studied using metal-organic vapor-phase epitaxy (MOVPE).

3D GaN structures offer several advantages, such as (i) improving the quality of multi-quantum wells (MQWs) due to the use of a selective-area epitaxial growth (SAG) technique¹³; (ii) reducing the quantum-confined Stark effect (QCSE) by using semi- and/or non-polar facets^{14,15}; (iii) varying the indium composition, for the broad spectrum, as the distance changes from the mask because of different diffusion lengths between indium and gallium adatoms^{16,17}; and (iv) enhanced light extraction efficiency because 3D GaN structures have textured surfaces¹⁸. Although some groups have demonstrated phosphor-free *broad* spectrum LEDs using 3D GaN structures grown by MOVPE, the realization of phosphor-free *white* LEDs has proved to be more challenging. In the previously reported results regarding phos-

phor-free white LEDs, a dramatic color coordinate shift was observed with changing injection current^{8,9,19,20}. For the purpose of a white light source, it is important to determine the origin of the color emission change and to achieve stable color emission.

Here, we report phosphor-free white LEDs that consistently emit white light with varying injection current. We intentionally designed the pattern and size to achieve double concentric, truncated pyramid fabricated (DCTP) structures with a truncated hexagonal pyramid surrounded by a hexagonal ring. We also investigated the origin of broadband emission and discuss the carrier injection efficiency for both spatially resolved micro-electroluminescence (μ -EL) and micro-photoluminescence (μ -PL).

MATERIALS AND METHODS

Growth and fabrication of DCTP LEDs

The *n*-GaN template was grown on a *c*-plane sapphire substrate by MOVPE. A 30 nm Si₃N₄ mask layer (Figure 1a) was fabricated on an *n*-GaN template by plasma-enhanced chemical vapor deposition and a UV-lithography technique. The Si₃N₄ mask layer patterned with openings of concentric circles consisting of a central hole and a ring is schematically illustrated in Figure 1a. The hole diameter (d_{hole}), inner ring diameter ($d_{\text{in_ring}}$), outer ring diameter ($d_{\text{out_ring}}$), and center-to-center distance (d_{pitch}) were 3, 9, 15, and 18 μm , respectively. After SAG of an *n*-GaN layer at 1040 °C on the above-patterned Si₃N₄ mask, we achieved DCTP structures. Figure 1b schematically illustrates a cross-sectional view of the DCTP-structured LEDs. The height

¹Department of Physics and KI for the NanoCentury, Korea Advanced Institute of Science and Technology, 291 Daehak-ro, Yuseong-gu, Daejeon 34141, Korea;

²Present address: Electronics and Telecommunications Research Institute (ETRI), 218 Gajeong-ro, Yuseong-gu, Daejeon 34129, Korea;

³Present address: The Laboratoire Nanotechnologies Nanosystèmes (LN2) - CNRS UMI-3463, Institut Interdisciplinaire d'Innovation Technologique (3IT), Université de Sherbrooke, 3000 boulevard Université, J1K 0A5, QC, Canada

Correspondence: YH Cho, Email: yhc@kaist.ac.kr

Received 14 May 2015; revised 18 September 2015; accepted 25 September 2015; accepted article preview online 26 September 2015

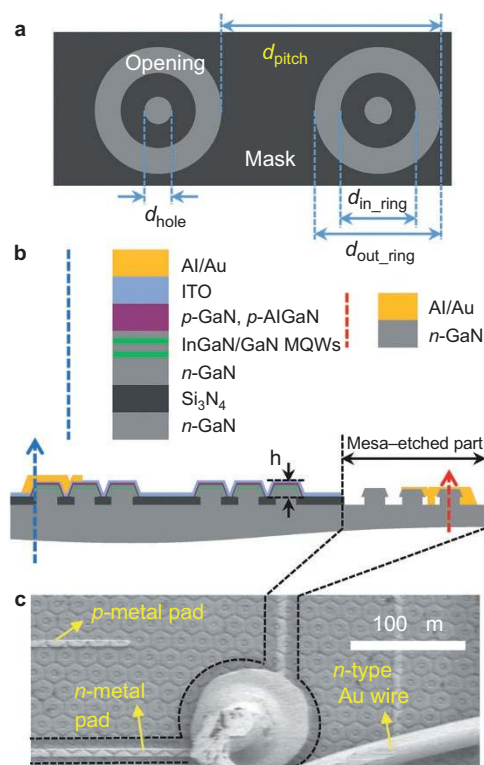


Figure 1 Device overview: (a) Top view mask schematic for SAG of DCTP LEDs. Dark gray and light gray areas are the Si_3N_4 mask and the opening part, respectively. (b) Cross-sectional view schematic and layer contents for both the LED and mesa-etched area (drawing not to scale). (c) Top view SEM image of the DCTP LED after the metal contact process.

of the n -GaIn DCTP structure is $1.3 \mu\text{m}$, which indicates that this structure has a lower aspect ratio compared with other types of 3D LEDs, such as rods, pyramids, and annular structures. Five pairs of InGaIn/GaN MQWs at $680^\circ\text{C}/850^\circ\text{C}$, p -AlGaIn, and p -GaIn layers were heteroepitaxially grown on n -GaIn DCTP structures. The V/III ratios of n -GaIn DCTP, InGaIn quantum wells, and GaIn quantum barriers were 60, 4000, and 1000, respectively. After mesa etching (LED chip size: $1.2 \text{ mm} \times 0.6 \text{ mm}$), a 55-nm thick (based on c -plane) indium tin oxide (ITO) layer was deposited on the DCTP LEDs. An Al/Au layer was used for n - and p -type electrodes. Figure 1c shows a top view scanning electron microscope (SEM) image of a DCTP LED after the Au wire bonding process, and black dotted lines indicate the mesa-etched part. To calculate the injected current density, the 3D geometrical area of p -GaIn was deduced by top view SEM image instead of the conventionally used 2D mesa-etched area. By considering the overall grown area on the mask and approximately 60° inclined semi-polar facets ($\{10\bar{1}1\}$: 61.9° ; $\{11\bar{2}2\}$: 58.4°)²¹, the p -GaIn area (i.e., 0.754 mm^2) of the 3D DCTP structure is approximately 1.05 times (see the Supplementary Information) larger than the 2D mesa area (i.e., 0.720 mm^2).

Cathodoluminescence and structural characterization

Spatial optical characterization on DCTP LED was performed at room temperature by cathodoluminescence (CL) (monoCL4, Gatan, Inc., Pleasanton, CA, USA) equipment connected to an SEM, where the acceleration voltage was 10 kV. A transmission electron microscopy specimen was prepared using the focused ion beam technique. The DCTP structure was also observed by spherical aberration-corrected,

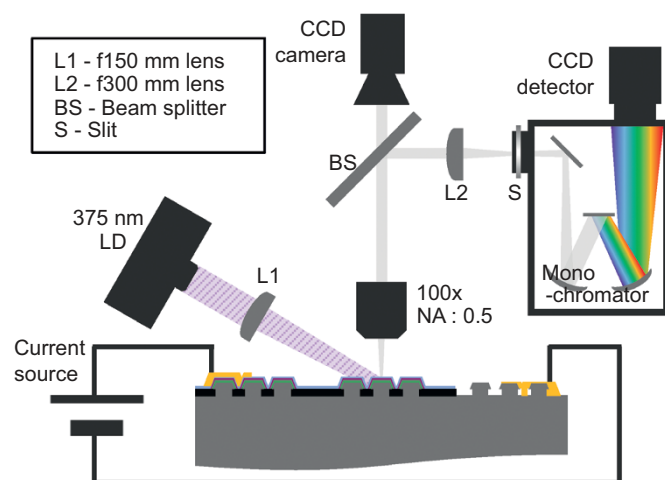


Figure 2 Setup schematic of μ -PL and μ -EL experiments. The DCTP structure was globally excited and locally detected for both μ -EL and μ -PL. The optics for the detection setup are shared, and both experiments were conducted at room temperature.

high-angle annular dark-field scanning transmission electron microscopy (HAADF-STEM) (JEM-ARM200F, JEOL, Ltd., Tokyo, Japan). To estimate the indium composition, the image contrast in the HAADF-STEM image scales and the atomic number, Z , were used²². Secondary ion mass spectrometry, which is frequently used to analyze the chemical composition in conventional 2D film, is not able to extract the indium molar fraction of the InGaIn layers in 3D structure LEDs. The values from energy-dispersive X-ray spectrometry are underestimated because the information of the InGaIn layer is detected together with that of the surrounding GaIn barrier. It is therefore likely that an analytical method for checking the indium composition deduced from the HAADF-STEM intensity has higher spatial resolution than the other measurement techniques.

μ -PL and μ -EL characterization

To investigate the spatial variation of the electron-hole injection efficiency in a single DCTP structure, μ -EL was conducted, and the results were compared with those from μ -PL at room temperature. Figure 2 schematically illustrates the experiment setup for μ -EL and μ -PL. The DCTP structure was globally excited and locally detected for both μ -EL and μ -PL. Resonant PL was also conducted to excite the InGaIn layer only. A microscope objective lens with a long working distance ($100\times$, $\text{NA} = 0.5$, Mitutoyo Corporation, Kawasaki, Japan) was used to spatially collect (approximately $1 \mu\text{m}^2$) the PL and EL emission from the DCTP structure in the normal direction. For global resonant excitation, a 375 nm semiconductor laser diode focused with a 150 mm macro lens and a source meter (Keithley 2400, Tektronix, Inc., Beaverton, OR, USA) were used for optical and electrical excitation, respectively. μ -PL and μ -EL spectra were measured using a monochromator (Acton SP2500, Princeton Instruments Corporation, Trenton, NJ, USA) in conjunction with a 2D, charge-coupled device detector with a grating of $300 \text{ lines mm}^{-1}$.

RESULTS AND DISCUSSION

DCTP structure geometries

DCTP structures have multifacets, including $\{10\bar{1}1\}$, $\{11\bar{2}2\}$, $\{0001\}$, and $\{11\bar{2}0\}$ facets, as shown in the top view SEM image presented in Figure 3 (and Figure 4a). As reported by Leung *et al.*²³, because the

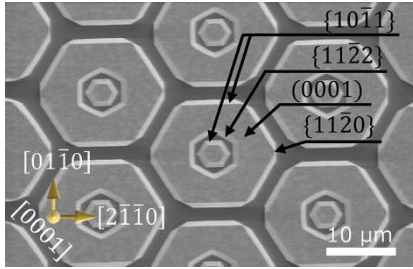


Figure 3 Top view SEM image of the DCTP LED after SAG. A DCTP structure has {11 $\bar{2}$ 0}, {0001}, {11 $\bar{2}$ 2}, and {10 $\bar{1}$ 1} facets.

concave growth front will be dominated by the fast-growing facet (i.e., the {11 $\bar{2}$ 2} facet), the diameter of the inner hexagonal ring (i.e., the concave growth front) decreases to 5 μ m, whereas the diameters of the inner truncated hexagonal pyramid and the outer hexagonal ring (i.e., the convex growth front) slightly increase during the growth of *n*-GaN. To fabricate phosphor-free white LEDs, several facets and harmonious proportions of these facets are required. Furthermore, it is important to make 3D structures with lower height for easier and stable fabrication; otherwise, a planarization step may be required to deposit a conducting and/or metal layer smoothly. We emphasize that the patterns and the sizes of the DCTP structures have been intentionally designed to achieve white color emission from a single 3D structure that has a lower height.

Emission characteristics of growth facets and their origin

Figure 4a shows the top view SEM image of a single DCTP structure where the yellow points indicate the excitation position for CL spectra plotted in Figure 4b. The GaN band-edge emission at 366 nm and a broadband emission at approximately 560 nm were observed for all CL spectra. The CL peak wavelength from the MQWs on the {10 $\bar{1}$ 1} and

{11 $\bar{2}$ 2} semi-polar facets was approximately 400 nm, whereas the emission from MQWs on the {0001} polar facet had a much longer wavelength of 560 nm. Furthermore, we found an additional CL emission with a peak wavelength of 470 nm from MQWs on the {11 $\bar{2}$ 0} facet. To clarify the origin of these emission peaks, monochromatic CL mapping images were taken at wavelengths of 410, 470, and 560 nm, as shown in Figure 4c–4e, respectively. The emission of MQWs on the {11 $\bar{2}$ 0} facet is clearly distinguished from MQWs on other facets (Figure 4d).

A bird's eye view SEM image is shown in Figure 5a. For further study, a transmission electron microscopy specimen, indicated by the red line in Figure 5a, was prepared. Figure 5b shows a HAADF-STEM image of a cross-sectional view of the specimen. InGaN/GaN MQWs and *p*-AlGaIn layers were clearly formed for both the {0001} and {11 $\bar{2}$ 0} facets. High magnification HAADF-STEM images of InGaN/GaN MQWs and *p*-AlGaIn on {0001}, {11 $\bar{2}$ 0}, and the joints between them are shown in Figure 5c, 5e, and 5d, respectively. The thicknesses of the InGaIn layers on {0001} and {11 $\bar{2}$ 0} are approximately 3.5 nm and 3 nm, respectively. The HAADF-STEM intensity of MQWs on {0001} and {11 $\bar{2}$ 0} facets was taken along the yellow and green arrow directions from Figure 5c and 5e and plotted in Figure 5f and 5g, respectively. The cyan minor grid of Figure 5f and 5g is of the same increment. The indium content inside the InGaIn layers on the {0001} and {11 $\bar{2}$ 0} facets was extracted by Equation (1):

$$I_{\text{InGaIn}} / I_{\text{GaN}} = \frac{xZ_{\text{In}}^{\epsilon} + (1-x)Z_{\text{Ga}}^{\epsilon} + Z_{\text{N}}^{\epsilon}}{Z_{\text{Ga}}^{\epsilon} + Z_{\text{N}}^{\epsilon}} \quad (1)$$

where *I* is the HAADF-STEM intensity, *x* is the elemental concentration in atomic percent, *Z* is the atomic number, and ϵ is a factor depending on the collection angle of the HAADF-STEM detector. The exponent was calibrated via energy dispersive spectroscopy²⁴, and the average value of the indium composition *x* was 0.232 ± 0.052 for InGaIn layers on the {0001} facet and 0.120 ± 0.009 for

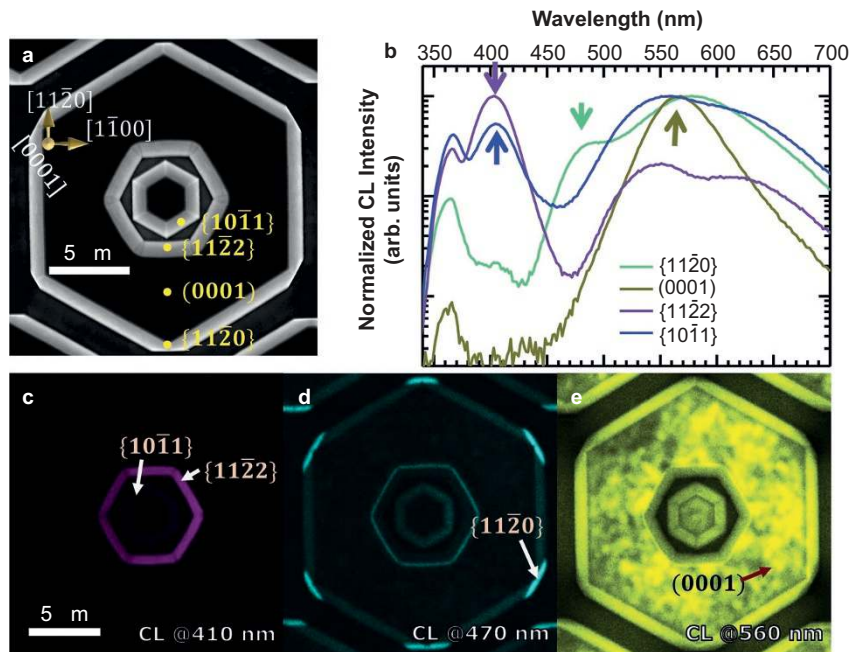


Figure 4 SEM image, spatially resolved CL spectra, and monochromatic CL images of the DCTP structure. (a) Top view SEM image of the DCTP structure. The yellow points indicate the excitation positions of the CL spectra. (b) The normalized CL spectra of InGaN/GaN MQWs on the {11 $\bar{2}$ 0}, {0001}, {11 $\bar{2}$ 2}, and {10 $\bar{1}$ 1} facets. The arrows indicate the specific emissions for each facet. Monochromatic CL mapping images taken at wavelengths of (c) 410 nm, (d) 470 nm, and (e) 560 nm.

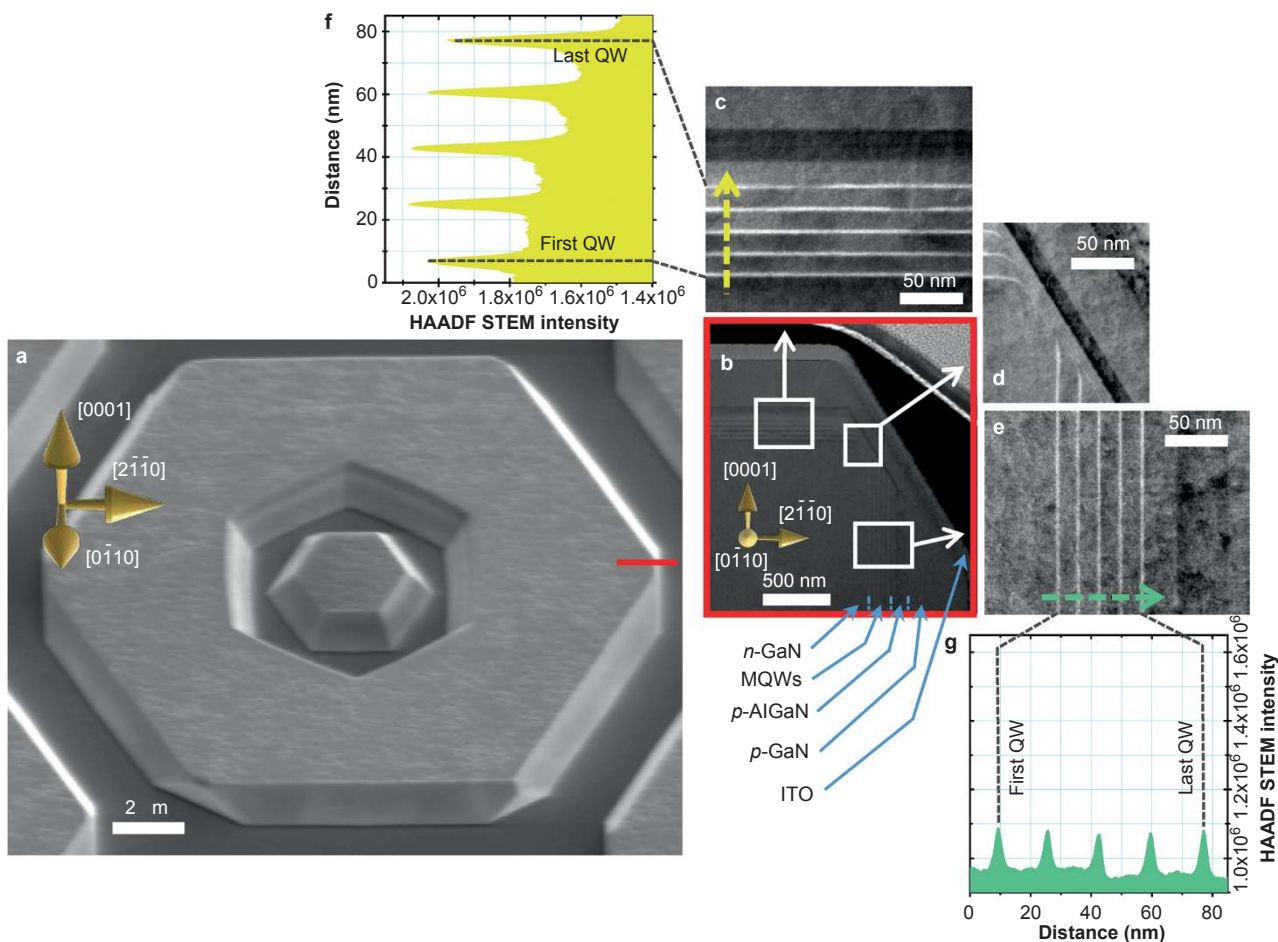


Figure 5 Structural characterization and indium composition analysis. (a) Bird's eye view SEM image of the DCTP structure. The red line indicates the position where the HAADF-STEM sample is inspected. HAADF-STEM images of (b) overview, (c) MQWs on the (0001) facet, (d) joint area, and (e) MQWs on the {1120} facet. Yellow and green arrows indicate the scan direction and its range for the HAADF-STEM intensity of (f) MQWs on the (0001) facet and (g) MQWs on the {1120}.

InGa_N layers on the {1120} facet. InGa_N MQWs on the (0001) facet have higher indium composition, greater well thickness, and a higher QCSE than those on {1120}. All factors push the QW emission to longer wavelength for InGa_N QWs on the (0001) facet.

Spatially resolved characterization method for carrier injection path

Panchromatic (PAN) μ -PL and μ -EL images are shown in Figure 6a and 6c, and a 2D image of the line scan spectrum is shown in Figure 6b and 6d, respectively. All images in Figure 6a–6d are normalized. Although the excitation power of the μ -PL (the injection current of μ -EL) experiments was adjusted from 10 mW to 30 mW (10 mA–100 mA with an LED chip size of 0.72 mm²), spatially resolved optical images and spectra were not significantly changed. Before obtaining the line-scan spectrum images, a slit was inserted in front of the monochromator to select the image area (between the black vertical lines in Figure 6a and 6c), which is parallel to [1120], whereas PAN images were taken without the slit.

First, PAN images under μ -PL and μ -EL (Figure 6a and 6c) conditions were compared. The PAN image under the μ -EL condition (Figure 6c) shows much higher intensity emission at the boundary between the (0001) and {101̄1} facets; however, the image under the μ -PL condition (Figure 6a) shows a relatively homogeneous emission

over the entire DCTP area. Because the sample and the detection setup were identical, similar internal quantum efficiency, light extraction efficiency, and emission collecting and detecting efficiency should be taken into account after the exciton generation, except for the carrier injection efficiency. We therefore found that the carrier injection efficiency is spatially different, whereas the photon injection is relatively uniform. The large spatial variation of the carrier injection efficiency is strongly related to the different thicknesses of the *p*-Ga_N layer, as shown in Figure 5b. Because of the growth rate change depending on the different facets, the *p*-Ga_N resistance between ITO and MQWs would vary locally. Consequently, higher hole injection efficiency occurs at a thinner *p*-Ga_N layer (i.e., an edge between a (0001) facet and a semi-polar or {1120} facet). Figure 6b and 6d shows the line-scan PL and EL spectra along the vertical positions. The emissions from 400 to 450 nm, 450 to 520 nm, and 520 to 640 nm indicate MQWs on semi-polar, {1120}, and (0001) facets, respectively. Unlike the μ -PL results (Figure 6b), the μ -EL (Figure 6d) spectral image has a brighter position at the boundary between the semi-polar or {1120} facets and the (0001) facet, as illustrated by the white dashed line in Figure 6d. The difference in the emission region from the (0001) facet (i.e., 520 nm–640 nm) between the μ -PL and μ -EL images is evidence that the hole injection efficiency depends on the *p*-Ga_N thickness over the whole area.

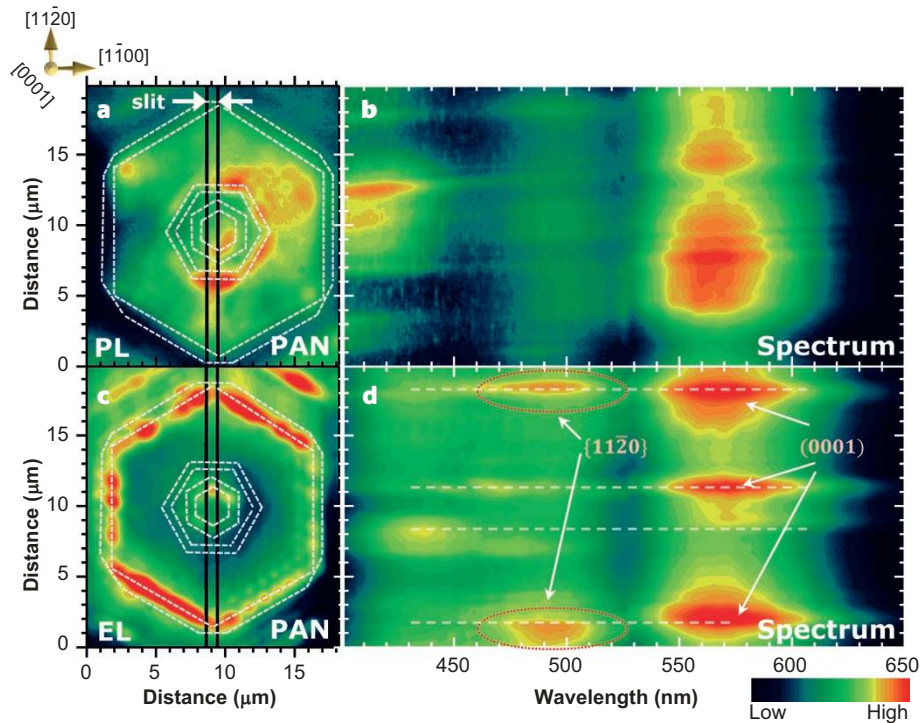


Figure 6 Optical characterization of the DCTP LEDs. (a) μ -PL PAN image and (b) line selected μ -PL spectrum image of the DCTP LEDs. (c) μ -EL PAN image and (d) line selected μ -EL spectrum image of the DCTP LEDs.

Ensemble luminescence characteristic of DCTP LEDs

From temperature-dependent PL data, a luminescence efficiency of approximately 3% was estimated for the entire spectrum (380 nm–700 nm) emitting from MQWs formed on various facets of DCTP LEDs (not shown here). Ensemble EL spectra were obtained under varying current from 10 mA to 100 mA for DCTP LEDs, as shown in Figure 7, and the Commission Internationale de l'Eclairage (CIE)-1931 coordinates of the corresponding current are plotted in the inset of Figure 7 and are presented in Table 1. Because the emission of MQWs on the $\{11\bar{2}0\}$ facet is clearly distinguished from MQWs on other facets, the single DCTP structure is not only able to emit white light but also reaches a high color rendering index (CRI) R_a ($\sim 75\%$), which was calculated from ensemble EL spectra (Figure 7). The CIE coordinates do not show significant changes with increasing current because at the low-current density region, due to the lesser thickness of the p -GaN layer, hole injection starts at the joint area (i.e., an edge between the (0001) facet and the semi-polar or $\{11\bar{2}0\}$ facet), as shown in Figure 5d. The area of hole injection then isotopically increases to the direction of each facet (i.e., semi-polar, $\{11\bar{2}0\}$, and (0001)) with increasing current. Because the portion of injected holes on each facet is not varied, DCTP LEDs were able to emit stable white light. A photographic image was taken and is displayed in the inset of Figure 7. The white emission properties (e.g., CIE coordinates and CRI value) can be adjusted by changing: (i) the size and design of the mask patterning; (ii) the growth time and V/III ratio of the n -GaN DCTP; and (iii) the growth conditions of the active layers (e.g., growth temperature, flow of group-III precursors).

CONCLUSIONS

We demonstrated electrically driven, phosphor-free white LEDs with DCTP structures grown by MOVPE. The patterns and sizes of the

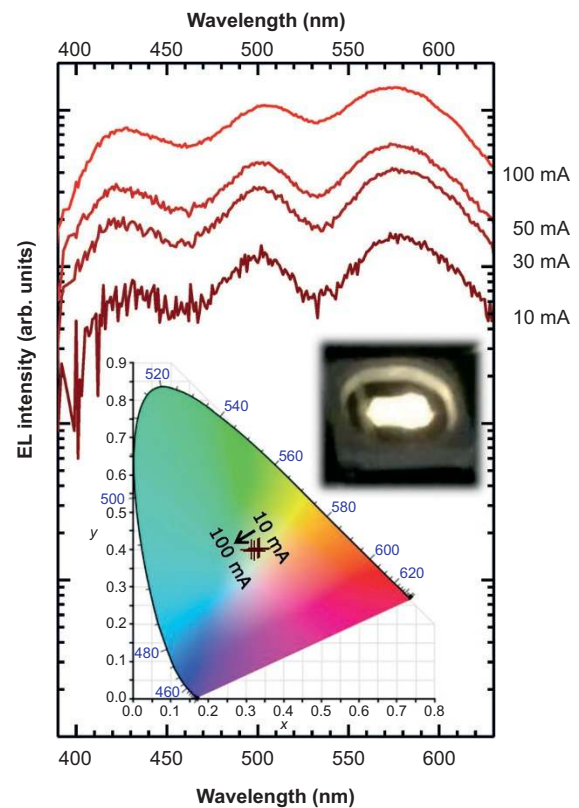


Figure 7 Current dependent ensemble EL spectra of the DCTP LEDs. The inset shows a photographic image and color coordinates for currents between 10 mA and 100 mA.

Table 1 CIE color coordinates of DCTP LEDs.

Current (mA)	<i>x</i>	<i>y</i>
10	0.362	0.391
30	0.361	0.390
50	0.350	0.385
100	0.343	0.390

DCTP structures have been intentionally designed to achieve white color emission from a single 3D structure that has a lower height. A DCTP structure has {10 $\bar{1}$ 1}, {11 $\bar{2}$ 2}, {11 $\bar{2}$ 0}, and (0001) facets that lead to high CRI white emission ($R_a \sim 75\%$). A CL experiment was conducted to determine the spatially resolved optical characterization. We confirm that each facet emits a different wavelength. HAADF-STEM images were taken to check the origin of the emission wavelength. We also conducted μ -PL and μ -EL measurements to assess the differences and found that the hole injection efficiency strongly depends on the thickness of the *p*-GaN layer for the 3D structure. This method could be adopted for checking the local hole injection for not only 3D structure LEDs but also 2D film LEDs. We successfully demonstrated a phosphor-free white LED, and the CIE color coordinates are relatively stable with varying current.

ACKNOWLEDGEMENTS

This work was supported by the National Research Foundation (NRF-2013R1A2A1A01016914, NRF-2013R1A1A2011750) of the Ministry of Education, the Industrial Strategic Technology Development Program (10041878) of the Ministry of Knowledge Economy, the Climate Change Research Hub of KAIST (Grant No.N01150041), and the GRC project of KAIST Institute for the NanoCentury. The authors wish to thank Soo Kun Jeon and his colleagues (Semicon Light Co., Ltd., Republic of Korea) for their help with the device fabrication process.

- 1 Nakamura S, Mukai T, Senoh M. Candela-class high-brightness InGaN/AlGaIn double-heterostructure blue-light-emitting diodes. *Appl Phys Lett* 1994; **64**: 1687–1689.
- 2 Ponce FA, Bour DP. Nitride-based semiconductors for blue and green light-emitting devices. *Nature* 1997; **386**: 351–359.
- 3 Schubert EF, Kim JK. Solid-state light sources getting smart. *Science* 2005; **308**: 1274–1278.
- 4 Nguyen HPT, Zhang SF, Connie AT, Kibria MG, Wang Q *et al*. Breaking the carrier injection bottleneck of phosphor-free nanowire white light-emitting diodes. *Nano Lett* 2013; **13**: 5437–5442.
- 5 Li YL, Gessmann T, Schubert EF, Sheu JK. Carrier dynamics in nitride-based light-emitting p-n junction diodes with two active regions emitting at different wavelengths. *J Appl Phys* 2003; **94**: 2167–2172.

- 6 Park IK, Kim JY, Kwon MK, Cho CY, Lim JH *et al*. Phosphor-free white light-emitting diode with laterally distributed multiple quantum wells. *Appl Phys Lett* 2008; **92**: 091110.
- 7 Soh CB, Liu W, Teng JH, Chow SY, Ang SS *et al*. Cool white III-nitride light emitting diodes based on phosphor-free indium-rich InGaIn nanostructures. *Appl Phys Lett* 2008; **92**: 261909.
- 8 Cho CY, Park IK, Kwon MK, Kim JY, Park SJ *et al*. InGaIn/GaN multiple quantum wells grown on microfacets for white-light generation. *Appl Phys Lett* 2008; **93**: 241109.
- 9 Wunderer T, Wang J, Lipski F, Schwaiger S, Chuvilin A *et al*. Semipolar GaInN/GaN light-emitting diodes grown on honeycomb patterned substrates. *Phys Stat Solidi C* 2010; **7**: 2140–2143.
- 10 Kim JH, Ko YH, Cho JH, Gong SH, Ko SM *et al*. Toward highly radiative white light emitting nanostructures: a new approach to dislocation-eliminated GaN/InGaIn core-shell nanostructures with a negligible polarization field. *Nanoscale* 2014; **6**: 14213–14220.
- 11 Ko YH, Song J, Leung B, Han J, Cho YH. Multi-color broadband visible light source via GaN hexagonal annular structure. *Sci Rep* 2014; **4**: 5514.
- 12 Wu K, Wei TB, Zheng HY, Lan D, Wei XC *et al*. Fabrication and optical characteristics of phosphor-free InGaIn nanopyramid white light emitting diodes by nanospherical-lens photolithography. *J Appl Phys* 2014; **115**: 123101.
- 13 Zhu D, Wallis DJ, Humphreys CJ. Prospects of III-nitride optoelectronics grown on Si. *Rep Prog Phys* 2013; **76**: 106501.
- 14 Chichibu SF, Uedono A, Onuma T, Haskell BA, Chakraborty A *et al*. Origin of defect-insensitive emission probability in In-containing (Al,In,Ga)N alloy semiconductors. *Nat Mater* 2006; **5**: 810–816.
- 15 Schwarz UT, Kneissl M. Nitride emitters go nonpolar. *Phys Stat Solidi RRL* 2007; **1**: A44–A46.
- 16 Tsuchiya T, Shimizu J, Shirai M, Aoki M. InGaAlAs selective-area growth on an InP substrate by metalorganic vapor-phase epitaxy. *J Cryst Growth* 2005; **276**: 439–445.
- 17 Feng W, Kuryatkov VV, Chandolu A, Song DY, Pandikunta M *et al*. Green light emission from InGaIn multiple quantum wells grown on GaN pyramidal stripes using selective area epitaxy. *J Appl Phys* 2008; **104**: 103530.
- 18 Fujii T, Gao Y, Sharma R, Hu EL, DenBaars SP *et al*. Increase in the extraction efficiency of GaN-based light-emitting diodes via surface roughening. *Appl Phys Lett* 2004; **84**: 855–857.
- 19 Tchoe Y, Jo J, Kim M, Heo J, Yoo G *et al*. Variable-color light-emitting diodes using GaN microdonut arrays. *Adv Mater* 2014; **26**: 3019–3023.
- 20 Hong YJ, Lee CH, Yoon A, Kim M, Seong HK *et al*. Visible-color-tunable light-emitting diodes. *Adv Mater* 2011; **23**: 3284–3288.
- 21 Scholz F. Semipolar GaN grown on foreign substrates: a review. *Semicond Sci Technol* 2012; **27**: 024002.
- 22 Amari H, Ross IM, Wang T, Walther T. Characterization of InGaIn/GaN epitaxial layers by aberration corrected TEM/STEM. *Phys Stat Solidi C* 2012; **9**: 546–549.
- 23 Leung B, Sun Q, Yerino CD, Han J, Coltrin ME. Using the kinetic Wulff plot to design and control nonpolar and semipolar GaN heteroepitaxy. *Semicond Sci Technol* 2012; **27**: 024005.
- 24 Ko SM, Gong SH, Cho YH. Nonlinear photonic diode behavior in energy-graded core-shell quantum well semiconductor rod. *Nano Lett* 2014; **14**: 4937–4942.



This work is licensed under a Creative Commons Attribution-NonCommercial-NoDerivs 4.0 Unported License. The images or other third party material in this article are included in the article's Creative Commons license, unless indicated otherwise in the credit line; if the material is not included under the Creative Commons license, users will need to obtain permission from the license holder to reproduce the material. To view a copy of this license, visit <http://creativecommons.org/licenses/by-nc-nd/4.0/>

Supplementary information for this article can be found on the *Light: Science & Applications*' website (<http://www.nature.com/lsa/>).